Global confinement and discrete dynamo activity in the MST reversed-field pinch*

S. Hokin,† A. Almagri, S. Assadi, J. Beckstead, G. Chartas, N. Crocker, M. Cudzinovic, D. Den Hartog, R. Dexter, D. Holly, S. Prager, T. Rempel, J. Sarff, E. Scime, W. Shen, C. Spragins, C. Sprott, G. Starr, M. Stoneking, and C. Watts
University of Wisconsin, Madison, Wisconsin 53706

R. Nebel
Los Alamos National Laboratory, Los Alamos, New Mexico 87545

(Received 10 December 1990; accepted 1 April 1991)

Results obtained on the Madison Symmetric Torus (MST) reversed-field pinch [Fusion Technol. **19**, 131 (1991)] after installation of the design poloidal field winding are presented. Values of $\beta_{\theta e0} \equiv 2\mu_0 n_{e0} T_{e0}/B_\theta^2(a) \sim 12\%$ are achieved in low-current ($I = 220$ kA) operation; here, n_{e0} and T_{e0} are central electron density and temperature, and $B_\theta(a)$ is the poloidal magnetic field at the plasma edge. An observed decrease in $\beta_{\theta e0}$ with increasing plasma current may be due to inadequate fueling, enhanced wall interaction, and the growth of a radial field error at the vertical cut in the shell at high current. Energy confinement time varies little with plasma current, lying in the range of 0.5–1.0 msec. Strong discrete dynamo activity is present, characterized by the coupling of $m = 1$, $n = 5$–7 modes leading to an $m = 0$, $n = 0$ crash (m and n are poloidal and toroidal mode numbers). The $m = 0$ crash generates toroidal flux and produces a small (2.5%) increase in plasma current.

I. INTRODUCTION

The Madison Symmetric Torus[1] (MST) is a large reversed-field-pinch (RFP) device ($R = 1.50$ m, $a = 0.52$ m) differing in design from its predecessors in a number of ways. It is comparable in size to the large, high-current RFP's currently being built (ZTH[2] at Los Alamos National Laboratory and RFX[3] at the Institute for Ionized Gases in Padua); however, its iron-core transformer, with a maximum flux swing of 2 Wb, limits the plasma current to values below 1 MA, making it a rather low current-density RFP. The 5 cm aluminum shell acts as a vacuum vessel, single-turn toroidal field coil and stabilizing shell—eliminating the vacuum liner and separate toroidal field coils present in other RFP devices. MST discharges have been maintained for up to 80 msec—over twice as long as in previous RFP experiments. This paper presents results obtained with the design poloidal field winding,[1] which was completed in January 1990. Results previously reported[4] were obtained with a temporary poloidal field winding.

The limiting values of plasma parameters obtained to date in MST are shown in Table I. Figure 1 displays waveforms for a long 450 kA discharge. MST is operated in ramped mode,[5] in which the RFP dynamo increases the toroidal flux by a factor of 3 while the plasma current increases to its maximum value. Both poloidal field and toroidal field crowbars are then fired to maintain a 10–20 msec flat top. Throughout the discharge, the reversal parameter $F = B_\phi(a)/\langle B_\phi \rangle$ and pinch parameter $\Theta = B_\theta(a)/\langle B_\phi \rangle$ are maintained constant (B_ϕ and B_θ are toroidal and poloidal magnetic field, respectively); values of Θ tend to be somewhat higher for a given F than on other RFP devices—for example, $\Theta = 1.85$ at $F = -0.15$. A notable aspect of the dynamo in MST is its tendency to increase the toroidal flux, after edge field reversal has begun, in discrete steps. This "discrete dynamo" has been observed in other RFP devices,[6–10] and is associated with magnetohydrodynamic (MHD) tearing instabilities;[11–13] it will be discussed in some detail in this paper.

MST is fueled with hydrogen using piezoelectric valves that are opened just before the discharge is created. This form of fueling, along with helium wall conditioning, allows the density to be varied throughout the range $3\times10^{-14} < I/N < 14\times10^{-14}$ A-m, where $N = \pi a^2 \langle n \rangle$ is calculated for a parabolic density profile. This range is typical for RFP experiments—the high-density boundary represents the onset of radiation in excess of the nominal level of 20% input power; the low-density boundary represents the difficulty in striking a discharge at low fill pressures.

The remainder of this paper is divided into three sections: Sec. II presents the arguments used to scale RFP confinement to a large, high-current fusion reactor and summarizes MST confinement results in the context of that scaling; Sec. III presents experimental results associated with the discrete dynamo; and Sec. IV is a summary.

TABLE I. Limiting values of plasma parameters achieved on MST in 1990.

I	<	600 kA
V_1	>	12 V
T_{e0}	<	500 eV
T_i	<	400 eV
$\bar{n}$	<	4×10^{13} cm^{-3}

* Paper 2I7, Bull. Am. Phys. Soc. **35**, 1942 (1990).
† Invited speaker.

 0899-8221/91/082241-06$02.00

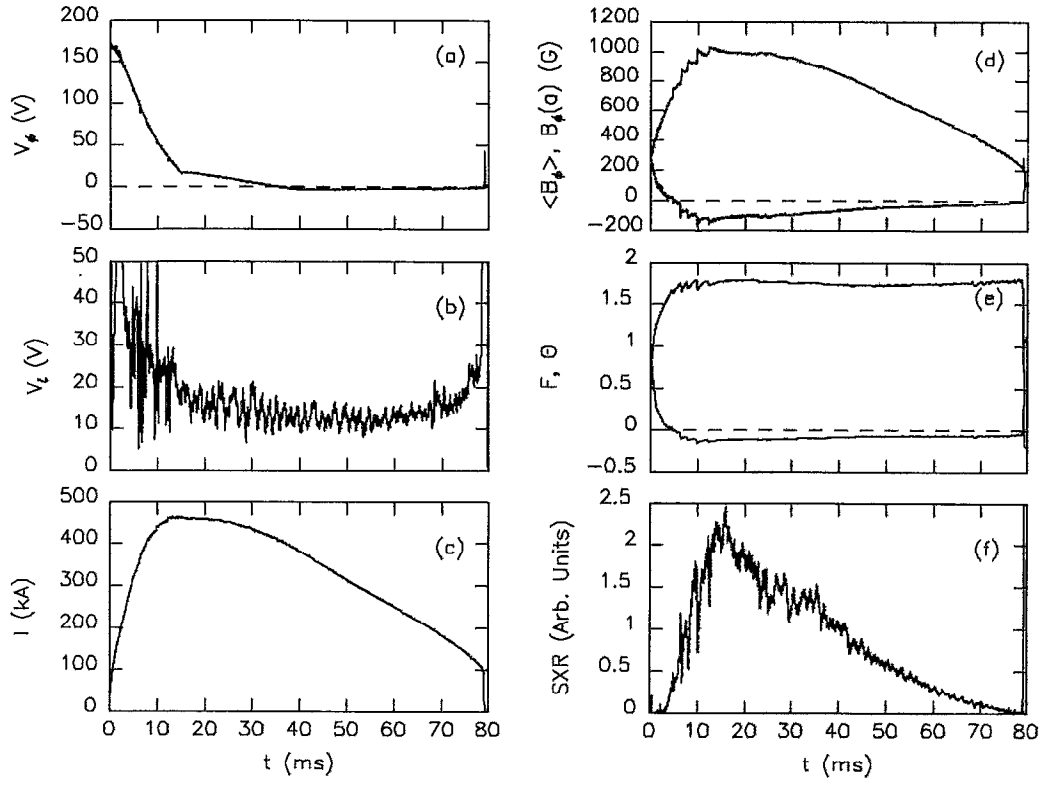

FIG. 1. Waveforms from a long MST discharge: Applied toroidal voltage (a), resistive loop voltage (b), plasma current (c), average and edge toroidal fields (d), reversal parameter and pinch parameter (e), and a central-chord soft x-ray signal (f).

II. MST CONFINEMENT

The RFP is attractive as a potential fusion reactor for three reasons: (1) It has high values of $\beta = 2\mu_0 p/B^2$, where p is the plasma pressure; (2) it has low magnetic field at the toroidal field coils (and therefore small forces); and (3) it may be Ohmically ignited in a compact size (the minor radius of MST is equal to that of the TITAN reactor design[14]). The good energy confinement hoped to be present in a large, high-current RFP is based on the premise, supported by some smaller RFP experiments,[15–17] that $\beta_\theta = 2\mu_0 \langle p \rangle / B_\theta^2(a)$ may be maintained at values of 10% or greater, independent of plasma current and size. MST is in a unique position to evaluate RFP confinement at large size, albeit at low current density.

To examine the dependence on plasma current and size, one simply needs to rewrite the formula for energy confinement time

$$\tau_E \equiv \tfrac{3}{2}\langle p \rangle \pi a^2 2\pi R / IV_l \qquad (1)$$

in terms of plasma current I, size a, and parameters that are independent of current and size. Here, R is the major radius of the device and V_l is the loop voltage, defined such that IV_l is the total power input to the plasma that is not inductively stored. One should note that, in an RFP, one can write $V_l = V_{\rm cl} + V_{\rm anom}$, where $V_{\rm cl}$ represents classical dissipation and electron heating, and $V_{\rm anom}$ represents anomalous power absorption processes.[18] It is also important to note that $V_{\rm cl}$ is roughly a factor of 4 greater in an RFP than in a tokamak of the same size and plasma parameters because of the fact that a large poloidal current is present in the RFP; this is sometimes termed the "screw-up" factor[19] and allows the RFP to have large Ohmic power densities even in the absence of an anomalous contribution.

To quantify the contribution of $V_{\rm anom}$ in a size-independent fashion, it is traditional to define the enhancement factor Z^*:

$$Z^* \equiv V_l / V_{\rm cl}(Z = 1). \qquad (2)$$

Since Z^* represents the enhancement of resistivity over that of a purely hydrogenic plasma of the same temperature, it includes both the effects of impurities ($Z_{\rm eff}$) and anomalous resistivity. The plasma pressure $\langle p \rangle$ may be eliminated from Eq. (1) by substituting β_θ, which, combined with Eq. (2), results in the form

$$\tau_E[\text{sec}] = 1.2 \times 10^{-3} a^2 \beta_\theta T_e^{3/2} / Z^* \ln \Lambda \ \ [\text{m,eV}]. \qquad (3)$$

Here, ln Λ is the Coulomb logarithm. Favorable scaling results from the increase in T_e with plasma current for constant β_θ and Z^*. This can be made explicit by replacing T_e with β_θ and I/N, using the assumptions $T_e = T_i$ and $\langle p \rangle = p_0/2$, where T_i is the ion temperature and p_0 is the plasma pressure in the center of the discharge. The first assumption is qualified for MST by charge–exchange measurements of T_i, which fall in the range $0.64 < T_i/T_{e0} < 1.1$ over a broad range of plasma conditions; the second assumption is not supported on MST because of the lack of profile information. This results in a form of τ_E in which all parameters other than I and a are independent of size and current:

$$\tau_E[\text{sec}] = 7.3\times10^{-13}a^2I^{3/2}$$
$$\times[\beta_\theta^{5/2}(I/N)^{3/2}/Z^*\ln\Lambda]\ \ [\text{m,A,A-m}]. \quad (4)$$

If β_θ can be maintained constant at fixed values of I/N and Z^*, the RFP reactor will achieve large values of τ_E at high plasma current.

Two experimental results influence the choice of I/N for optimizing confinement. The first, shown in Fig. 2, is that the loop voltage enhancement tends to be smallest at high density (low I/N). MST and other RFP experiments[17,20] follow the relation $Z^* \sim 10^{14} I/N$ [A-m]. The second result, displayed in Fig. 3, is that β_θ tends to be highest at high density (low I/N). This has also been noted in other RFP experiments.[15,20] Although Fig. 3 displays $\beta_{\theta e0} = 2\mu_0 n_0 T_{e0}/B_\theta^2(a)$ calculated from the central electron temperature and density, ion temperature measurements indicate that the total β_θ is likely to follow the same trend.

With the assumption that values of $\beta_\theta = 10\%$, $Z^* = 3$, and $I/N = 3\times10^{-14}$ A-m may be maintained independent of plasma current and size, one arrives at a scaling relation for energy confinement in the RFP:

$$\tau_E[\text{sec}] = 0.029a^2I^{3/2}\ \ [\text{m,MA}]. \quad (5)$$

Using this relation, MST is projected to achieve $\tau_E = 6$ msec at $I = 0.8$ MA, ZTH is projected to achieve $\tau_E = 40$ msec at $I = 4$ MA, and the TITAN design would have $\tau_E = 550$ msec at $I = 18$ MA. MST plays an important role in testing this relation at large size and moderate current.

Values of $\beta_{\theta e0}$ obtained with a central Thomson scattering measurement are displayed in Fig. 4 for a set of discharges in which density and plasma current were varied. One can see that, on the average, $\beta_{\theta e0}$ tends to degrade with increasing plasma current. The highest values consistently obtained are $\beta_{\theta e0} = 12\%$ at $I = 220$ kA, $I/N = 4\times10^{-14}$ A-m. Since these are central measurements, they do not account for profile effects; data from ZT-40M[21] indicate that the pressure profile broadens with increasing current, such that β_θ may not decrease as drastically as $\beta_{\theta e0}$. Nevertheless,

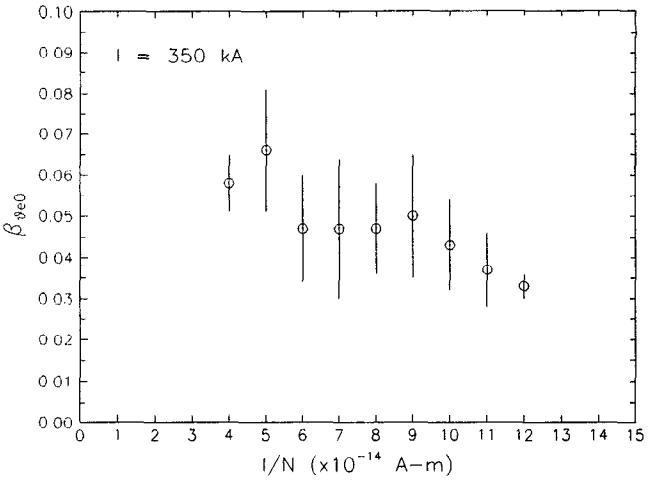

FIG. 3. Values of $\beta_{\theta e0} = 2\mu_0 n_0 T_{e0}/B_\theta^2(a)$ derived from central electron temperature and density measured with a Thomson scattering diagnostic at a fixed plasma current of 350 kA. A parabolic density profile is assumed in calculating the line density N.

even a completely flat pressure profile would keep the bulk of the high-current points below 10%. The lower $\beta_{\theta e0}$ values at high current may partly be due to the fact that the high-current discharges do not have the low I/N values reached in the low-current cases.

Energy confinement times, calculated using $\beta_{\theta e0}$ with the assumptions $T_i = T_e$ and $\langle p\rangle = p_0/2$, are displayed in Fig. 5. Rather than displaying an $I^{3/2}$ increase, τ_E does not vary greatly with plasma current. This is due to the degradation of $\beta_{\theta e0}$ with increasing current as well as the fact that the high-current discharges tend to have larger loop voltages. The observed value of $\tau_E \sim 1$ msec at $I = 220$ kA, $I/N = 4\times10^{-14}$ A-m is consistent with Eq. (5).

The lack of adherence to the RFP scaling relation equation (5) at high currents in MST may be due to a number of factors: Lack of validity of the profile assumption

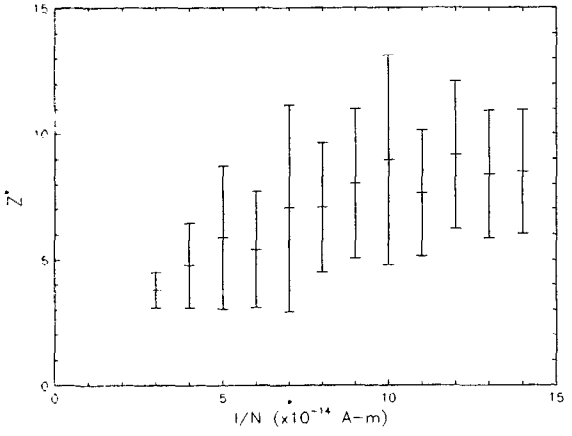

FIG. 2. Values of Z^* for a set of discharges sorted into bins of constant I/N. The plasma current ranged from 180–580 kA and the central density ranged from 7×10^{12} to 3×10^{13} cm^{-3}. The electron temperature and density were measured with a Thomson scattering diagnostic in the center of the discharge. A parabolic density profile is assumed in calculating the line density N.

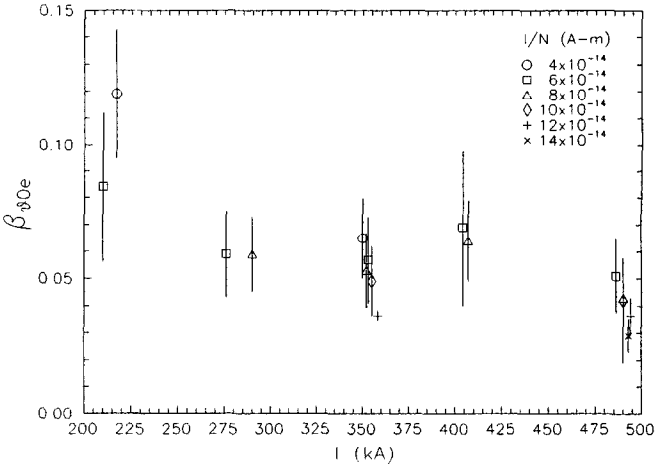

FIG. 4. Values of $\beta_{\theta e0} = 2\mu_0 n_0 T_{e0}/B_\theta^2(a)$ derived from central electron temperature and density measured with a Thomson scattering diagnostic for various values of plasma current and density.

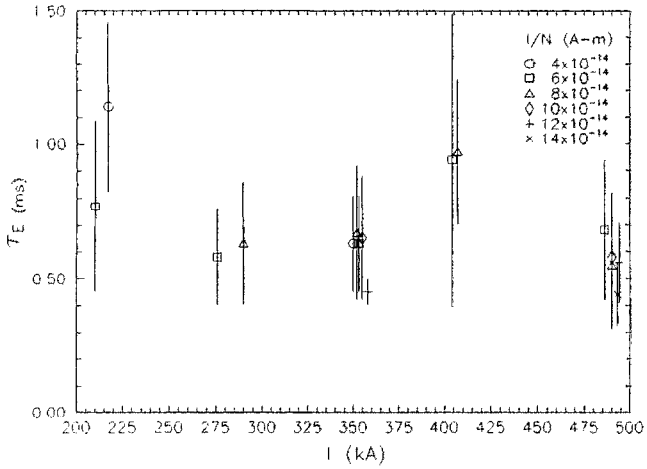

FIG. 5. Values of $\tau_E = 3n_0 T_{e0} 4\pi^2 a^2 R / 2IV_1$ derived from central electron temperature and density measured with a Thomson scattering diagnostic for the set of discharges displayed in Fig. 4.

$\langle p \rangle = p_0/2$, inadequate fueling (resulting in larger I/N values), enhanced wall interaction (resulting in larger Z_{eff} and loop voltage), and the appearance of an $m = 1$ radial field error at the vertical cut in the shell. The effect of this field error is demonstrated in Fig. 6. High-current discharges have shortened length and enhanced loop voltages due to the growth of this $m = 1$ field error. Both passive and active field correction schemes are being pursued to correct this field error; frozen hydrogen pellet injection and additional graphite armoring will be utilized to address the fueling and wall interaction issues; and installation of an 11-channel far infrared interferometer array, a scanning charge–exchange analyzer, and a multipoint Thomson scattering system will allow determination of the pressure profile.

III. DISCRETE DYNAMO ACTIVITY

The RFP, like the tokamak, exhibits $m = 1$ MHD tearing instabilities (here, m is the poloidal mode number and n is the toroidal mode number). In the RFP, this activity is associated with the conversion of poloidal flux to toroidal flux—the MHD dynamo. In the case of MST, as can be seen in Fig. 1, the dynamo often generates toroidal flux in discrete events, which have been measured to correspond to the coupling of resonant internal modes. Following a brief summary of RFP tearing mode physics, this section will present experimental observations associated with the discrete dynamo activity in MST.

Figure 7 displays typical $q(r) = rB_\phi/RB_\theta$ profiles for a tokamak and an RFP with the aspect ratio of MST. Unlike the tokamak, which tends to have a single resonant $m = 1$, $n = 1$ mode in the interior, the RFP has several resonant $m = 1$ modes, such as $n = 5,6,7$ for the case of MST. Tokamak internal disruptions may eliminate the $m = 1$, $n = 1$ resonance by raising $q(0)$ to values greater than unity; RFP internal disruptions are thought to stabilize, but not remove, the resonant $m = 1$ modes by raising $q(0)$.[22]

The many resonant $m = 1$ modes present in the RFP provide fertile ground for nonlinear coupling. In general, modes may couple with mode numbers satisfying the relation

$$(m,n) + (m',n') \rightarrow (m - m', n - n') + (m + m', n + n'), \tag{6}$$

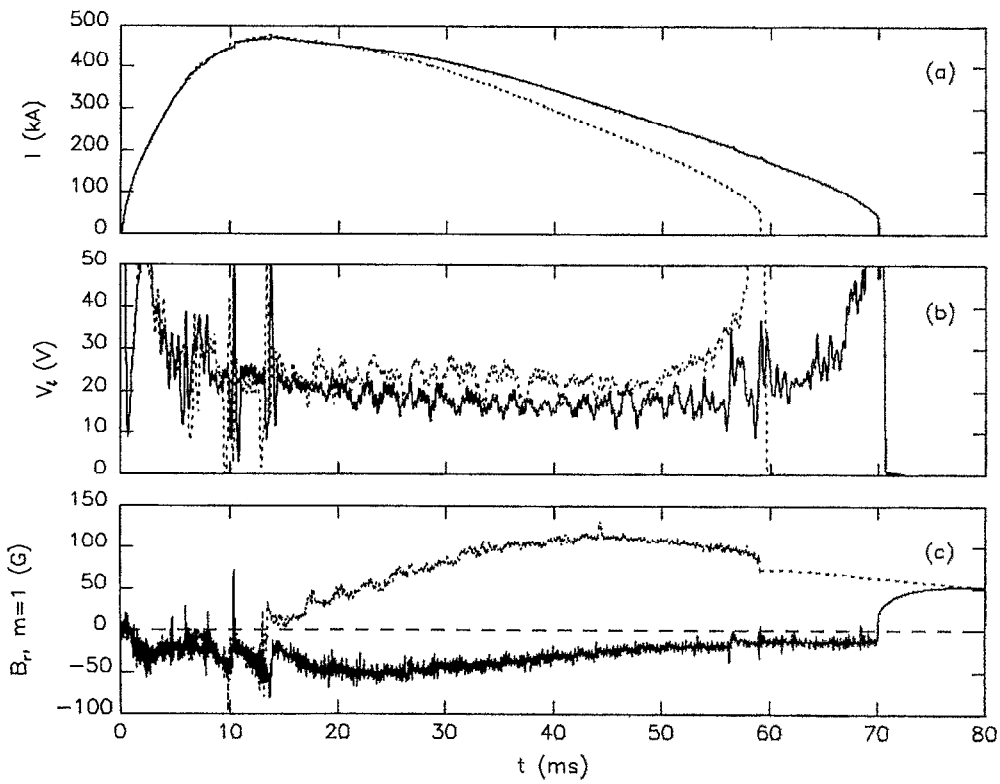

FIG. 6. Plasma current (a), resistive loop voltage (b) and vertical field ($m = 1$ sine component) at the vertical cut in the shell (c) for discharges with (dotted) and without (solid) growth of an $m = 1$ field error.

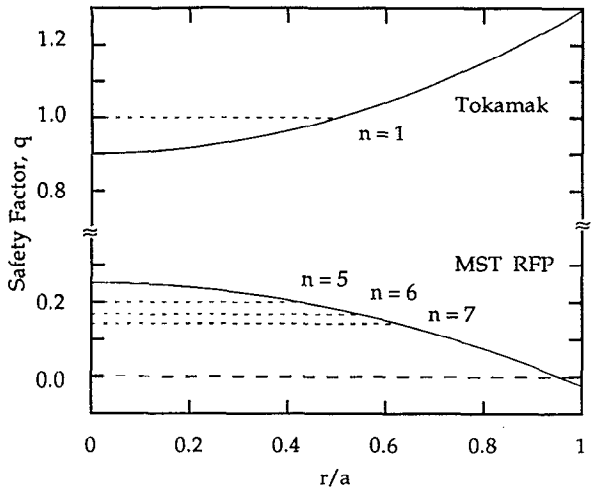

FIG. 7. Typical profiles of $q(r) = rB_\phi/RB_\theta$ for a tokamak and an RFP with an aspect ratio $R/a = 3$ corresponding to MST.

which accounts for the generation of toroidal flux ($m - m' = 0, n - n' = 0$) if one considers the self-coupling of $m = 1$ modes. MST has a number of diagnostic arrays that are used for mode studies: Two poloidal and one toroidal array of edge magnetic coils (allowing measurement of modes with numbers up to $m = 8$, $n = 32$), a "dense" array of edge magnetic coils spaced 1 cm apart for local measurement of high m,n mode amplitudes, and an array of surface barrier diodes that measure soft x-ray (SXR) emission through 7.6 μm Be filters and are used for tomographic reconstruction of emissivity in the interior. Bispectral analysis[23] of magnetic signals is used to identify nonlinear coupling between modes.

One of the issues connected with the discrete dynamo is the question of underlying continuous dynamo activity—is the period between discrete dynamo events influenced by continuous generation of toroidal flux, or does the toroidal flux simply decay at a rate given by the plasma resistivity? Figure 8 displays the results of a transport simulation using the RFPBURN code,[24] in which the decay of the toroidal flux and edge toroidal field are successfully modeled with a resistivity profile

$$\eta(r) = \eta_0 (\tfrac{1}{4} + \tfrac{3}{4} e^{-7(r/a)^2})^{-3/2}, \tag{7}$$

where η_0 is given by the Spitzer formula with the measured central temperature $T_{e0} = 250$ eV and $Z_{\text{eff}} = 2$. The code maintains a toroidal voltage that matches the measured experimental value. The resistivity profile given by Eq. (7) would represent, if classical, a very peaked electron temperature profile, which is not expected; it likely incorporates an anomalous contribution to resistivity. It appears, however, that the effect of a continuous dynamo, if it exists, is to raise the plasma resistivity to the anomalous level measured; the fields decay on the magnetic diffusion time scale given by that resistivity.

In many cases, $m = 1$ modes are observed to rotate between discrete dynamo events.[7,10] Mode analysis of the full toroidal magnetic array indicates that the 10–20 kHz rotating $m = 1$ disturbance is composed primarily of $n = 5,6,7$ components. These components rise in amplitude prior to the dynamo event, at which time nonlinear coupling, which obeys Eq. (6), is observed to occur by means of bispectral mode analysis. The $m = 1$ rotation is evident in Fourier–Bessel tomographic reconstruction[25] of soft x-ray signals, as displayed in Fig. 9. The $m = 1$ modes sometimes become stationary, at which time the $m = 1$ radial field at the vertical gap in the shell grows, as shown in Fig. 6. The longest discharge durations are achieved when the $m = 1$ modes continue to rotate.

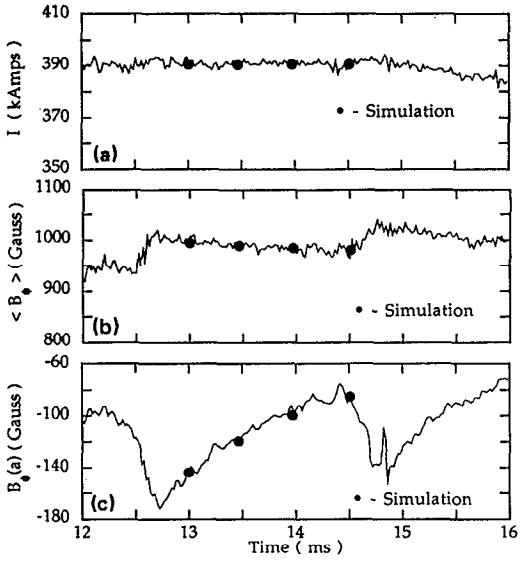

FIG. 8. Plasma current (a), average toroidal field (b), and toroidal field at the plasma edge (c) in a time interval encompassing two discrete dynamo events, along with RFPBURN simulation results.

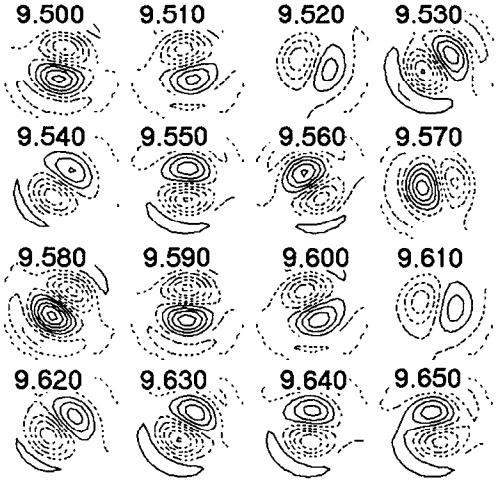

FIG. 9. Contours of soft x-ray emissivity reconstructed from signals that have been digitally high-pass filtered ($f_b = 5$ kHz) to emphasize the $m = 1$ structure rotating with frequency around 12 kHz during a period between discrete dynamo events. Positive/negative levels are indicated with solid/dashed contours. The times in the discharge are shown in msec. Fourier–Bessel tomographic reconstruction is used with two radial modes and $m = 0,1$.

An unexpected aspect of the discrete dynamo is the sudden increase in plasma current of typically 2.5% during the $m = 0$ crash. As the dynamo is expected to convert poloidal flux to toroidal flux, this observation appears contradictory; however, a redistribution of toroidal current can increase the net toroidal current while decreasing the net poloidal flux. For a given toroidal current density perturbation profile, $\delta j_\phi(r)$, the resulting change in plasma current and poloidal flux Ψ_θ may be written

$$\Delta I \propto \int_0^a dr\, r\delta j_\phi(r), \tag{8}$$

and

$$\Delta \Psi_\theta \propto \int_0^a dr \frac{1}{r} \int_0^r dr'\, r' \delta j_\phi(r'). \tag{9}$$

The dynamo crash is expected to stabilize tearing modes by flattening $j_\phi(r)$; i.e., δj_ϕ is expected to be negative near the plasma center and positive at outer radii. Test δj_ϕ profiles may be easily constructed that have this characteristic and render $\Delta I > 0$ with $\Delta \Psi_\theta < 0$, due to the different r-weighting of the integrands in Eqs. (8) and (9).

IV. SUMMARY

MST operation is characterized by strong discrete dynamo events that occur from the time of toroidal field reversal up to or past the time of peak current; these events are responsible for the increase in toroidal flux during this time, with resistive decay of the toroidal flux and edge toroidal field occurring during the period between them. The presence of unstable $m = 1$ modes, with characteristic toroidal mode numbers $n = 5$–7, and nonlinear coupling leading to an $m = 0$ crash are consistent with MHD tearing mode predictions.[11–13]

In its first nine months of design operation, MST has achieved 80 msec pulse lengths with values of $\beta_{\theta 0}$ as high as 12% at low values of I and I/N with a corresponding energy confinement time $\tau_E = 1$ msec. Energy confinement at high current may be limited by the appearance of an $m = 1$ radial field error at the vertical gap in the shell associated with the locking of $m = 1$ modes, enhanced wall interaction associated with high-current operation, and inadequate fueling to achieve low I/N values at high current. These issues are currently being addressed on MST.

[1] R. N. Dexter, D. Kerst, T. W. Lovell, S. C. Prager, and J. C. Sprott, Fusion Technol. **19**, 131 (1991).
[2] H. Driecer, in *Proceedings of the International School of Plasma Physics Workshop on Physics of Mirrors, Reversed Field Pinches and Compact Tori*, Varenna, Italy (Societa Italiana di Fisica, Bologna, 1987), Vol. 1, p. 331.
[3] G. Malesani, in Ref. 2, p. 359.
[4] S. C. Prager, A. F. Almagri, S. Assadi, J. A. Beckstead, R. N. Dexter, D. J. Den Hartog, G. Chartas, S. A. Hokin, T. W. Lovell, T. D. Rempel, J. S. Sarff, W. Shen, C. W. Spragins, and J. C. Sprott, Phys. Fluids B **2**, 1367 (1990).
[5] J. A. Phillips, D. A. Baker, R. F. Gribble, and C. Munson, Nucl. Fusion **28**, 1241 (1988).
[6] R. G. Watt and R. A. Nebel, Phys. Fluids **26**, 1168 (1983).
[7] G. A. Wurden, Phys. Fluids **27**, 551 (1984).
[8] R. G. Watt and E. M. Little, Phys. Fluids **27**, 784 (1984).
[9] H. Y. W. Tsui and J. Cunnane, Plasma Phys. Controlled Fusion **30**, 865 (1988).
[10] R. J. Hayden and B. Alper, Plasma Phys. Controlled Fusion **31**, 193 (1989).
[11] E. J. Caramana, R. A. Nebel, and D. D. Schnack, Phys. Fluids **26**, 1305 (1983).
[12] R. A. Nebel, E. J. Caramana, and D. D. Schnack, Phys. Fluids B **1**, 1671 (1989).
[13] K. Kusano and T. Sato, Nucl. Fusion **27**, 821 (1987).
[14] R. W. Conn, F. Najmabadi, R. A. Krakowski, K. R. Schultz, and D. Steiner, in *Plasma Physics and Controlled Nuclear Fusion Research, 1988* (IAEA, Vienna, 1989), Vol. 3, p. 315.
[15] T. Shimada, Y. Yagi, Y. Hirano, K. Hattori, I. Hirota, Y. Kondoh, Y. Maejima, K. Saito, S. Shiina, and K. Ogawa, in *Plasma Physics and Controlled Nuclear Fusion Research, 1988* (IAEA, Vienna, 1989), Vol. 2, p. 457.
[16] K. Sato, T. Amano, Z. X. Chen, H. Arimoto, S. Yamada, A. Nagata, K. Yokoyama, Y. Kamada, A. Matsuoka, S. Masamune, H. Shindo, K. Saito, H. Murata, H. Oshiyama, S. Shiina, and T. Tamaru, in *Plasma Physics and Controlled Nuclear Fusion Research, 1986* (IAEA, Vienna, 1987), Vol. 2, p. 413.
[17] B. Alper, S. Martini, and S. Ortolani, Nucl. Fusion **26**, 1256 (1986).
[18] T. R. Jarboe and B. Alper, Phys. Fluids **30**, 1177 (1987).
[19] J. C. Sprott, Phys. Fluids **31**, 2266 (1988).
[20] H. A. B. Bodin, in Ref. 2, p. 307.
[21] P. Weber, in *Proceedings of the International School of Plasma Physics Workshop on Physics of Alternative Confinement Schemes*, Varenna, Italy (Societa Italiana di Fisica, Bologna, in press).
[22] V. Antoni, P. Martin, and S. Ortolani, Plasma Phys. Controlled Fusion **29**, 279 (1987).
[23] D. E. Smith and E. J. Powers, Phys. Fluids **16**, 1373 (1973).
[24] K. A. Werley, R. A. Nebel, and G. A. Wurden, Phys. Fluids **28**, 1450 (1985).
[25] Y. Nagayama, J. Appl. Phys. **62**, 2702 (1987).